



## The Effect of Friction Stir Processing on Microstructure and Mechanical Properties of Al6061-T6 Aluminium Alloy

Sayede Razieh Anvari<sup>1,2,\*</sup>, Fathallah Karimzadeh<sup>3</sup>, Mohammad Hossien Enayati<sup>3</sup>

<sup>1</sup>Assistant Professor, Daneshpajoohan Higher Education Institute, Isfahan, Iran.

<sup>2</sup>Ph.D. Graduated from Isfahan University of Technology, Isfahan, Iran.

<sup>3</sup>Professor, Isfahan University of Technology, Isfahan, Iran.

Received: 10 May 2023; Accepted: 10 June 2023

\*Corresponding author email: [sr.anvari1365@gmail.com](mailto:sr.anvari1365@gmail.com)

### ABSTRACT

In this research, the influence of friction stir processing (FSP), on structural and mechanical properties of Al6061-T6 was investigated. Friction stir processing with tool rotational rate ( $\omega$ ) of 630, 800 and 1000rpm and traveling speed ( $v$ ) of 50,100,160 and 200mm/min was employed on 13mm thick Al6061-T6. Results indicated that FSP decreases grain size from 78 $\mu$ m to 6 $\mu$ m because of the dynamic recrystallization. The finest grain size was obtained at the rotational rate of 630 rpm and traveling speed of 100 mm/min. Results have recommended that when the ratio of  $\omega/v$  was less than 5(rpm/mm.min<sup>-1</sup>), due to inadequate heat input, microscopic voids were produced in nugget zone (NZ). Microhardness and tensile strength in the stir zone decreased, but elongation raised compared to those for the base metal. This is due to the loss of hardening precipitates during FSP. With increasing the tool travelling speed, grain size in nugget NZ and mechanical properties were improved. The best mechanical properties at NZ have been obtained at  $\omega=630$  rpm and  $v=100$  mm/min due to the finest grain size.

**Keywords:** Friction stir processing, Al6061-T6, Grain size, Mechanical Properties.

### 1. Introduction

Aluminum and its alloys are suitable in many industries such as aircraft, automobile industry, structural applications and food packing due to their high strength to weight ratio and corrosion resistance. Aluminum–Magnesium–Silicon (Al–Mg–Si) indicated as 6XXX series alloys have advantages such as strength, excellent formability, good corrosion resistance, weld ability and low cost, comparing to other aluminum alloys [1-3]. Al6061 alloy is an age hardenable alloy possessing

with increased strength due to the precipitation of Mg-Si phase upon solution and artificial aging. Alloys of this class are extensively working in marine structures, pipes, storage tanks and aircraft applications [4,5]. Many researchers studied the effects of friction stir processing (FSP) on structures and mechanical properties of aluminum and magnesium alloys. FSP is a solid-state process in which a specially designed rotating cylindrical tool, including of a pin and a shoulder, with constant rotational and traveling speed is plunged into the

sheet. The tool is then traversed in the wanted direction. Fig. 1 shows schematic picture of FSP.

The rubbing of the rotating shoulder causes heat, which softens the material (below the melting temperature of the sheet) and with the mechanical stirring produced by the pin; the material within the processed zone undergoes great plastic deformation producing a dynamically recrystallized fine grain structure. In spite of the large number of studies that are being conducted to advance FSP technology, the effects of FSP on various mechanical and microstructural properties are still in need for further surveys. Zeinelabdeen et al. investigated friction stir surface processing of 6061 aluminium alloy. In their work a pinless tool with a fixed traveling speed and different rotational rate were used. In this work corrosion resistance and microhardness of Al-6061 alloy were studied[7]. In another research, Mehta et al. studied friction stir processing on wear behavior of Al-6061 T6 alloy. In this study, the variables of FSP were number of passes and direction of processing passes. Results showed the enhanced surface properties of the processed samples due to grain refinement, breaking and

better dispersion of precipitates after processing[8]. In fact, due to the lack of comprehensive studies to investigate the effect of both tool rotational rate and travelling speed of FSP on macrostructural and microstructural evaluations and also mechanical properties of Al6061-T6 aluminium alloy, so in this research the evolution of Al6061 after FSP with different parameters is investigated.

## 2. Experimental Procedure

The aluminum alloy which is studied in the present work was a thick sheet of Al6061-T6 alloy with a thickness of 13mm. The chemical composition and mechanical properties of this alloy are listed in Table 1 and 2. The direction of FSP was normal to the rolling direction. A Non-consumable tool used in this study was made of hot-work steel H13. The tool dimensions are indicated in Fig.2. Process was done at different rotational and travelling speeds that are listed in Table 3. All the samples were taken from the cross section of the processed area at the middle of the sheet thickness. Sample preparation contains grinding, polishing and etching. Microstructural analysis was

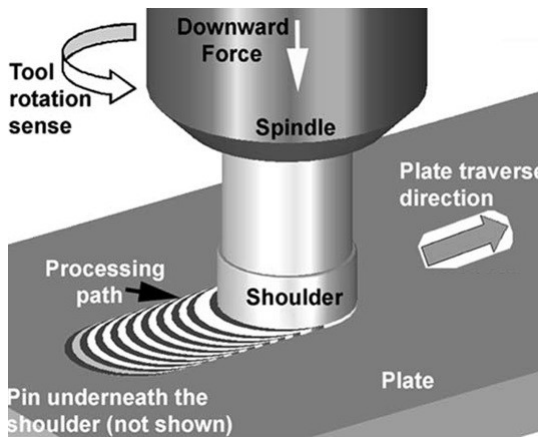


Fig. 1- Schematic drawing of FSP[6].

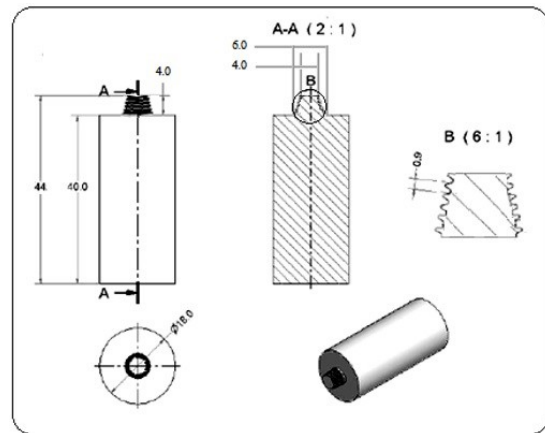


Fig. 2- FSP tool dimensions (all dimensions are in mm).

Table 1- Chemical composition (wt%) of as-received Al6061-T6 alloy

Microhardness	Elongation at Break	Ultimate Tensile Strength	Tensile Yield Strength
5 HV±97	%1.24±13	3.24 MPa±324	2.2MPa±300

Table 2- Mechanical properties of as-received Al6061-T6 alloy

Si	Fe	Cu	Mn	Mg	Cr	Zn	B	Al
0.3	0.5	0.1	0.03	0.35	0.03	0.1	0.06	Bal
0.7	Max	Max	Max	0.8	Max	Max	Max	

carried out with an optical microscope. A Vickers microhardness testing machine was employed for measuring the hardness. Tensile tests were carried out at strain rate of 2.5 mm.min<sup>-1</sup> strain rate. Fig.3 illustrates the tensile specimen geometry.

### 3. Results and Discussion

#### 3.1. Macrostructural Evaluation

The macrostructure of all specimens after FSP was analyzed (Table 4). With changing  $\omega/v$  ratio some defects appeared. Results indicate that when  $\omega/v$  ratio is  $\leq 5$ , defects like porous would be observed. Frigaard and et al. [10] suggested equation 1 for heat input as a result of FSP.

$$q = \frac{4}{3}\pi^2\mu P\omega R^3 \quad (\text{eq. 1})$$

Where  $q$  is net power,  $\mu$  is friction coefficient,  $P$  is pressure,  $\omega$  is rotational speed and  $R$  is the radius

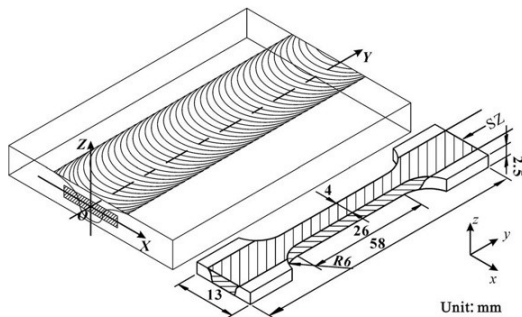


Fig. 3- Geometry of tensile specimen [9].

of pin. According to equation 1 heat input per length ( $Q$ ) is calculated from equation 2.

$$Q = \frac{4\pi^2\mu P\omega R^3}{3v} \quad (\text{eq. 2})$$

Where  $v$  is travelling speed[11]. Under constant  $R$  condition, equation 2 could be changed to equation 3[11].

$$Q \propto \frac{P\omega}{v} \quad (\text{eq. 3})$$

As seen,  $\omega/v$  ratio affects  $Q$ , so that with reducing  $\omega/v$  heat input would be decreased. Heat input in the nugget zone effects metal flow. At higher travelling speed, heat input reduces and low metal flow causes defect formation. When  $\omega/v$  ratio was more than 5, specimens included no defects.

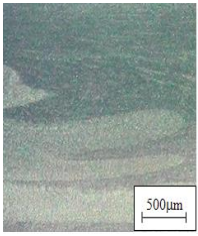
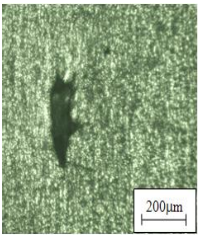
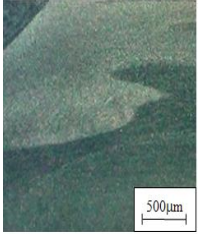
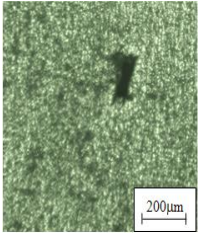
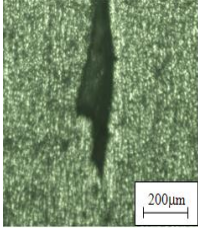
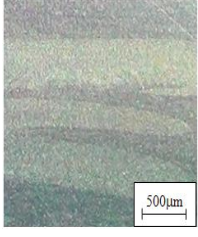
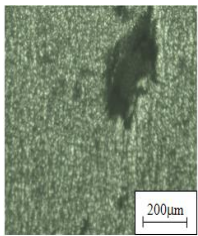
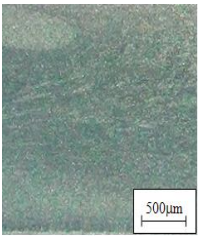
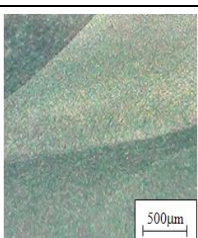
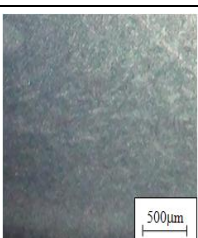
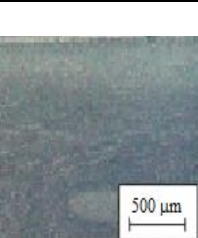
#### 3.2. Microstructural Evaluation

Microstructure of Al6061-T6 before FSP is displayed in Fig.4. Grain size is about 78  $\mu\text{m}$ . Fig.5 shows microstructure of alloy after friction stir processing, this structure includes four different regions; (a) unaffected base metal, (b) heat affected zone (HAZ), (c) thermo-mechanically affected zone (TMAZ) and (d) nugget zone(NZ). The formation of these regions is affected by the material flow behavior under the action of rotating non-consumable tool [12]. The nugget zone experiences high strain and is prone to recrystallization. Immediately, at its side is the TMAZ which ends at the tool shoulder, where the

Table 3- Rotational and traveling speeds used for FSP.

Number of test	$\omega(\text{rpm})$	$v(\text{mm} / \text{min})$
A1	630	50
A2		100
A3		160
A4		200
A5	800	50
A6		100
A7		160
A8		200
A9	1000	50
A10		100
A11		160
A12		200

Table 4- Effect of parameters on formation of defects

Sample	Parameters	Macrostructure	Sample	Parameters	Macrostructure
A1	$\omega = 630 \text{ rpm}$ $v = 50 \text{ mm/min}$ $\omega/v = 12.6$		A7	$\omega = 800 \text{ rpm}$ $v = 160 \text{ mm/min}$ $\omega/v = 5$	
A2	$\omega = 630 \text{ rpm}$ $v = 100 \text{ mm/min}$ $\omega/v = 6.3$		A8	$\omega = 800 \text{ rpm}$ $v = 200 \text{ mm/min}$ $\omega/v = 4$	
A3	$\omega = 630 \text{ rpm}$ $v = 160 \text{ mm/min}$ $\omega/v = 3.9$		A9	$\omega = 1000 \text{ rpm}$ $v = 50 \text{ mm/min}$ $\omega/v = 20$	
A4	$\omega = 630 \text{ rpm}$ $v = 200 \text{ mm/min}$ $\omega/v = 3.2$		A10	$\omega = 1000 \text{ rpm}$ $v = 100 \text{ mm/min}$ $\omega/v = 10$	
A5	$\omega = 800 \text{ rpm}$ $v = 50 \text{ mm/min}$ $\omega/v = 16$		A11	$\omega = 1000 \text{ rpm}$ $v = 160 \text{ mm/min}$ $\omega/v = 6.25$	
A6	$\omega = 800 \text{ rpm}$ $v = 100 \text{ mm/min}$ $\omega/v = 8$		A12	$\omega = 1000 \text{ rpm}$ $v = 200 \text{ mm/min}$ $\omega/v = 5$	

material experiences fewer strains and strain rates as well as lower maximum temperatures. This region is often identified by a pattern of grain distortion that suggests shearing and flow of material about the rotating tool. The grain distortion may lead to fragmentation and formation of refined, equiaxed grains near the interface between the TMAZ and the nugget zone. Beyond the TMAZ, the heat affected zone (HAZ) experiences only a thermal cycle and finally; the base material surrounds the HAZ [13,14]. However it could be identified two regions that are called advancing side and retreating side. Their formation depends on how the tool rotates and moves. Microstructural details of NZ for all friction stir processed samples are displayed in Fig. 6. Nugget microstructures are refined when compared with the base material.

In the nugget zone for different rotational and travelling speed, grain sizes change between 6 to 15.5µm. Some dark precipitates could be observed in the whole nugget zone. These precipitates are Mg<sub>2</sub>Si [15]. The equiaxed grains in the stir zone are formed by dynamic recrystallization [16]. Results indicate that grain size decreases with

increasing travelling speed (Fig.7). For samples with  $\omega/(v \leq 5)$  defects are developed. The grain sizes for these samples were not considered. According to equation 3 and 4, heat input and processing temperature decrease with increasing travelling speed.

$$\frac{T}{T_m} = k \left( \frac{\omega^2}{v \times 10^4} \right)^\alpha \quad (\text{eq. 4})$$

Where T is maximum temperature in NZ, T<sub>m</sub> is melting point of alloy, α and k are constant [17]. Thus, at higher travelling speed less time is available for grain growth. The decrease in grain size with increasing traveling speed can also be attributed to greater straining of the metal which in turn motivates more strain-free nucleation sites [18]. The greater the nucleation rate, the more competitive the grain growth and therefore the finer the final grain size will be [18]. According to equations 4 and 5 higher tool rotational speed consequences in a higher temperature and higher strain rate.

$$\dot{\epsilon} = \frac{R_m 2\pi r_e}{L_e} \quad (\text{eq. 5})$$

Where  $\dot{\epsilon}$  is strain rate, r<sub>e</sub> and L<sub>e</sub> are effective radius and length of recrystallization region, respectively [19].

Higher strain rate and lower temperature result finer grain size. The strain rate and deformation temperature are often incorporated into a single parameter the Zener-Holloman parameter (Z), which is explained as:

$$Z = \dot{\epsilon} \exp \left( \frac{-Q}{RT} \right) \quad (\text{eq. 6})$$

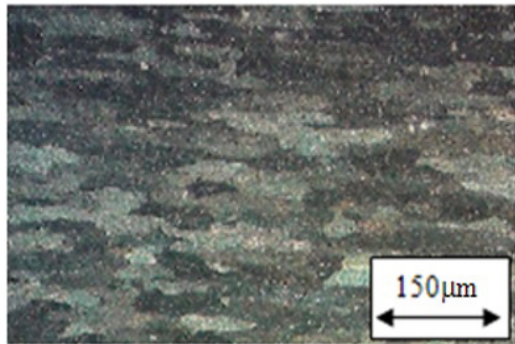


Fig. 4- Microstructure of as-received Al6061-T6.

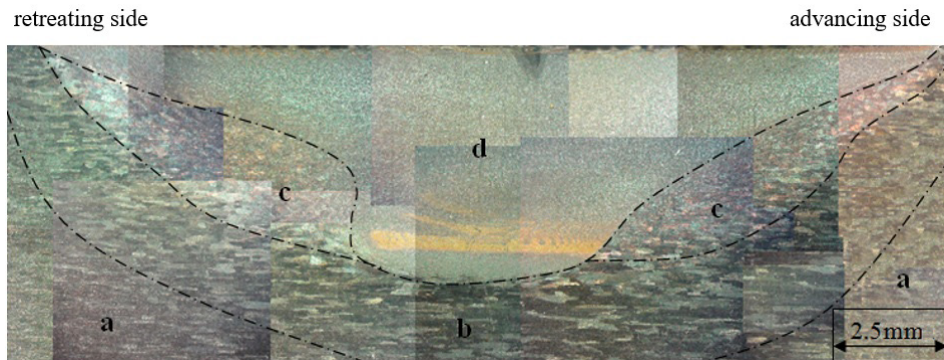


Fig. 5- Different regions of FSP: (a) unaffected base metal; (b) heataffected zone (HAZ); (c) thermo-mechanically affected zone (TMAZ); (d) nugget zone(NZ).

Where  $Q$  is the lattice self-diffusion activation energy which is 142 (kJ/mol) for Al [20]. Measured temperatures, strain rate, Zener-Holloman parameter and grain size for some samples are

listed in Table 5.

Furuet al.(1992) have studied grain sizes in aluminium alloys for a wide range of conditions and indicated that the relationship between grain

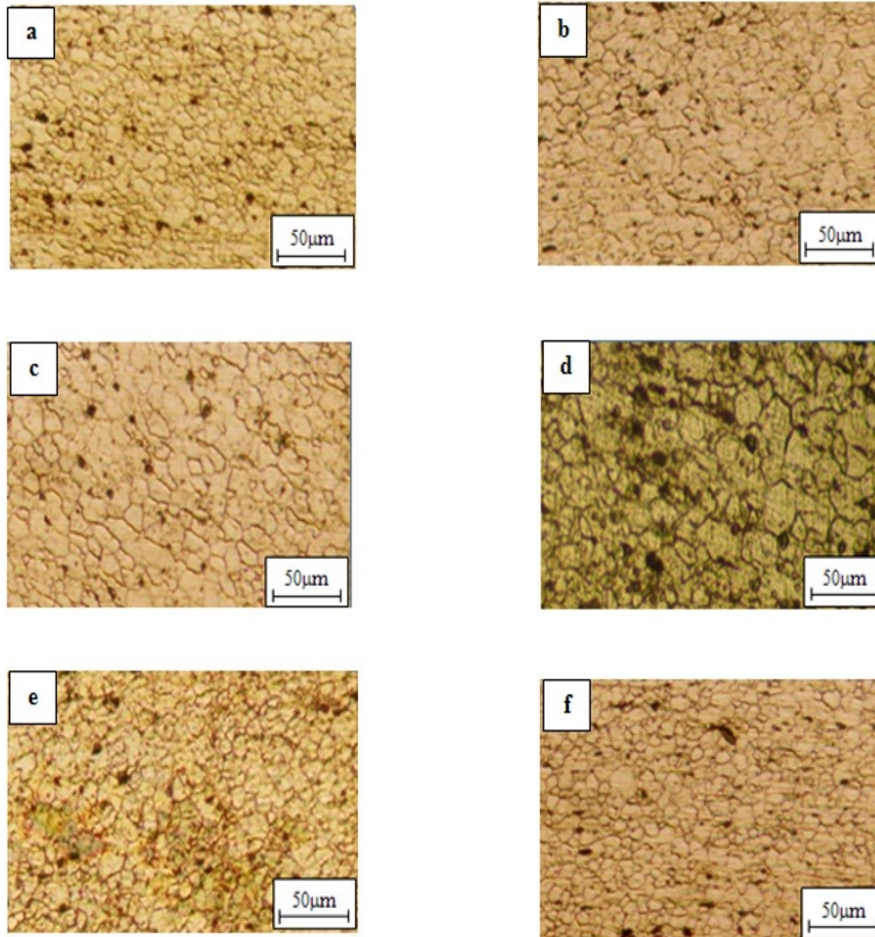


Fig. 6- Effect of rotational and traveling speed on microstructure of nugget zone. (a) $\omega=630$  V=50,(b) $\omega=800$ V=50,(c) $\omega=800$  V=100,(d)  $\omega=1000$  V=50,(e)  $\omega=1000$  V=100,(f) $\omega=1000$  V=160.

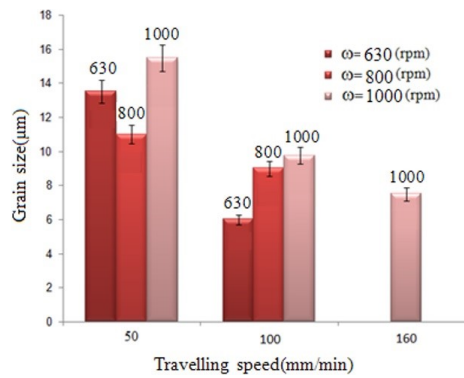


Fig. 7- Effect of traveling speed and rotational speed on grain size of NZ.

size (D) and Zener-Holloman parameter (Z) for  $10^{13} < Z < 10^{17}$  can be expressed empirically as:

$$D = k_1 + k_2 \log Z \quad (\text{eq. 7})$$

Where  $k_1$  and  $k_2$  are constants [21]. Fig. 8 displays the relationship between Zener-Holloman parameter and grain size. According to this figure by increasing Z, grain sizes decrease. Equation 6 shows that deformation temperature has more effect on Z, proposing that deformation temperature has a more effect than strain rate on the grain size.

### 3.3. Microhardness Measurements

For all specimens, microhardness decreases when approaching the TMAZ. The average hardness of the nugget zone (NZ) was found to be significantly lower than the hardness of the base alloy. There is a zone outside the nugget which has the lower hardness value. The difference of the microhardness values in the processed area and parent material is due to the dissimilarity between the microstructures of the base alloy and nugget zone. The lowest hardness value was observed at the retreating side. Similar observations were also made by Harris et al. and Scialpi et al. [22, 23]. The loss of T6 condition, which occurs during processing, is expected to decrease the mechanical strength reflected in the drop of hardness. As described in the literature, in alloys such as Al6061 the main strengthening precipitate is  $\beta''$ -Mg<sub>2</sub>Si<sub>6</sub>, which is stable at temperatures lower than [24]. This precipitate exists in the unaffected base material but is absent in the nugget and in the

HAZ. Results show that through FSP in nugget zone temperatures are over than during heating (Fig.9) so that  $\beta''$  is easily dissolved.

This  $\beta''$  precipitate is the main responsible for hardening. Svensson et al.[15] reported that no other fine scale precipitation was found in the nugget, while in the HAZ precipitation of  $\beta'$ -Mg<sub>2</sub>Si occurred on the Al-Mn-Si dispersoids. On cooling, precipitation of  $\beta'$  is easier than  $\beta''$ , and since the  $\beta'$  precipitates have less strengthening effect compared to  $\beta''$ , a lower hardness is obtained. The  $\beta'$  will act as nucleation sites for the precipitates. Following the diagram of continuous cooling precipitation (CCP) presented by Grong [24], in the HAZ where temperatures are near or less than 300 C the precipitation of  $\beta'$  is very high, and as a result the transition from  $\beta''$  to  $\beta'$  occurs by dissolution. In the NZ, the temperature is expected to be higher, therefore the Mg-Si precipitates go into solution. On cooling, the time for precipitation is limited, thus only a small volume fraction of the  $\beta'$  precipitates are formed in the weld nugget [25]. The nugget hardness recovery is due to recrystallization of a fine grain structure as displayed in Fig.10.

Fig.11 shows the effect of traveling speed and rotational speed on microhardness of the nugget zone after Friction stir processing. Results indicate that the maximum hardness at NZ has been obtained at and  $\omega=630$  rpm and  $v=100$ mm/min. The finer grain size obtained using these parameters.

### 3.4. Tensile tests

The stress/strain records of FSP specimens and

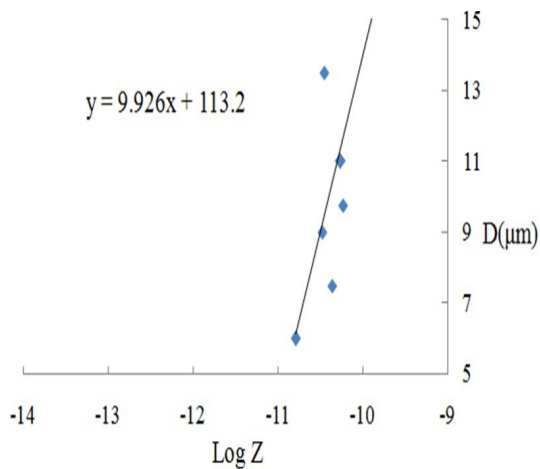


Fig. 8- Relationship between Zener-Holloman parameter and grain size.

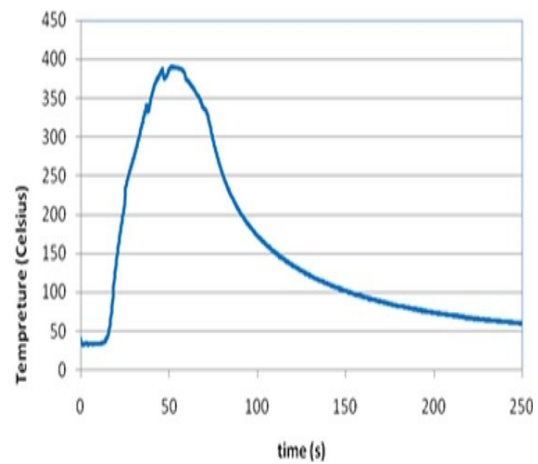


Fig. 4- Temperature profile during FSP ( $\omega=800$   $v=50$ ).

base material specimens are displayed in Fig.12. Friction stir processed samples present the lower yield and ultimate stresses but higher elongation than base material. These results are due to disappearing of some strengthening precipitates with FSP. With increasing travelling speed, yield and ultimate stress increase because of decrease in grain size. Lack of  $\beta$ -Mg<sub>2</sub>Si<sub>6</sub> precipitates due to

FSP results higher plastic deformation and higher elongation than base material. Fracture in the tensile tests took place in this softened region, which happened to be the weakest point of the specimen. The fracture surfaces of tensile tested specimens are characterized using SEM to understand the failure patterns. The fractographs taken from the tensile fractured surfaces of different slices are displayed in

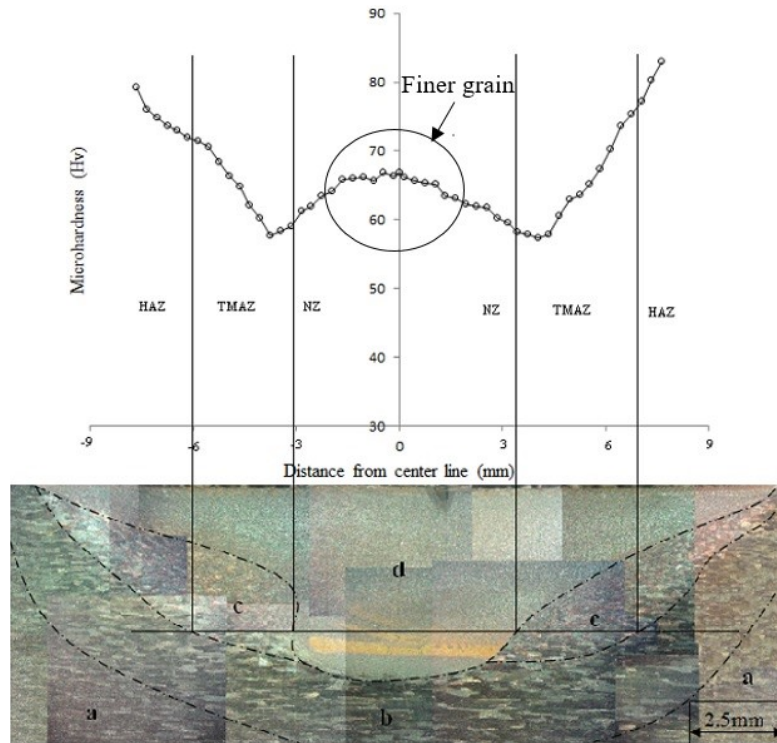


Fig. 10- Microhardness profile after friction stir processing with  $\omega = 800$  v=200.

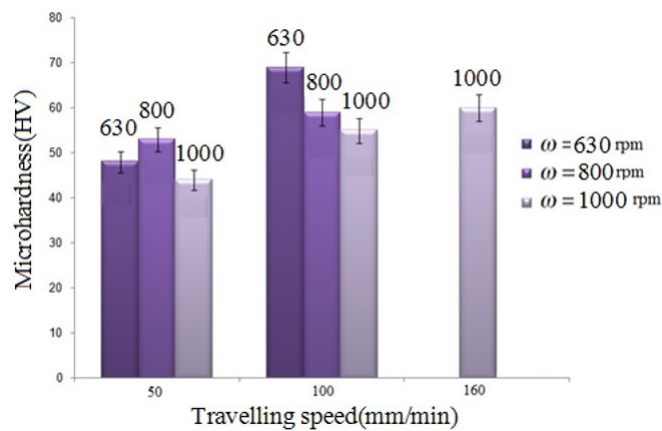


Fig. 11- Effect of traveling speed and rotational speed on microhardness of nugget zone after friction stir processing.

Fig. 13. All the fractured surfaces consist of dimples having various sizes and forms, which means the ductile failure.

4. Conclusions

In this research, the microstructure and mechanical properties of FSP samples from a plate

of Al6061-T6 were studied. The main results of this research can be summarized as follows:

1-Microhardness, yield and ultimate stresses decreased while elongation increased after FSP.

2-With increasing the tool travelling speed, grain size in NZ decreased and mechanical properties were improved.

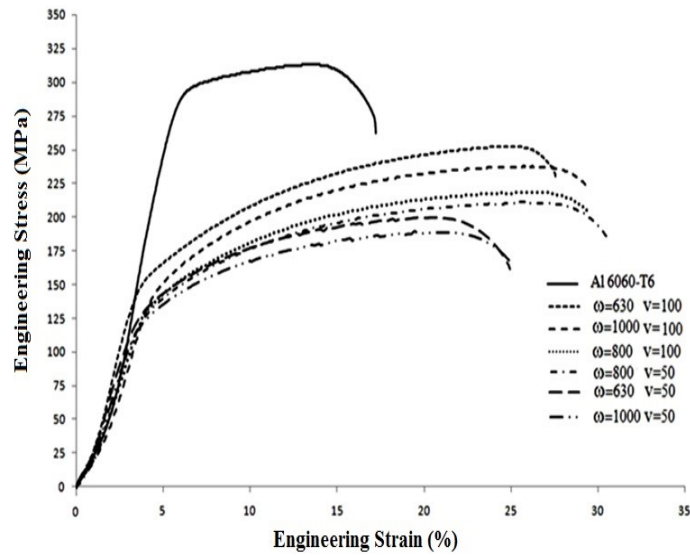


Fig. 12- Tensile properties for base metal and FSP samples.

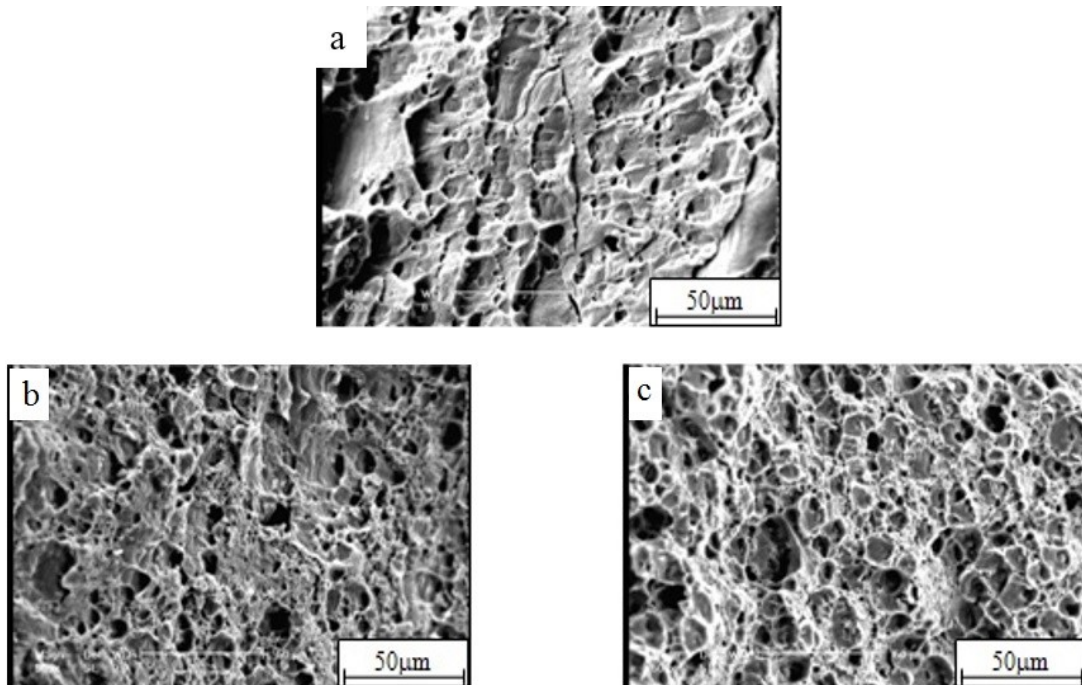


Fig. 13- Tensile fractured surfaces of (a)as-received Al 6061, and FSPed samples (b)ω =800 V=50, (c) ω =800 V=200.

3-The best mechanical properties at NZ have been obtained at  $\omega=630$  rpm and  $v=100$  mm/min.

## References

1. Das S. Design and Weight Optimization of Aluminium Alloy Wheel. International Journal of Scientific and Research Publication. 2014;4:1-12.
2. Raj RJ, Selvam PP, Pughalendi M. A Review of Aluminum Alloys in Aircraft and Aerospace Industry. Journal of Huazhong University of Science and Technology. 2021; 50: 1-10.
3. Basavegowda N, Mandal TK, Baek KH. Bimetallic and Trimetallic Nanoparticles for Active Food Packaging Applications: A Review. Food and Bioprocess Technology. 2020; 13:30–44.
4. Chandla NK, Kant S, Goud MM. Mechanical, tribological and microstructural characterization of stir cast Al-6061 metal/matrix composites-a comprehensive review. Sadhana. 2021; 46: 1-38.
5. Ogunsanya OA, Akinwande AA, Balogun OA, Romanovski V, Kumar M S. Mechanical and damping behavior of artificially aged Al 6061/TiO<sub>2</sub> reinforced composites for aerospace applications. Particulate Science and Technology. 2022; 41:196-208. DOI:10.1080/02726351.2022.2065652
6. Charit I, Mishra RS. Low temperature super plasticity in a friction-stir-processed ultrafine grained Al-Zn-Mg-Sc alloy. Acta Materialia. 2005;53: 4211–4223.
7. Zainelabdeen IH, Al-Badour FA, Adesina AY, Suleiman R, Ghaith FA. Friction stir surface processing of 6061 aluminum alloy for superior corrosion resistance and enhanced microhardness. International Journal of Lightweight Materials and Manufacture. 2023; 6: 129-139.
8. Mehta KM, Badheka VJ. Effect of friction stir processing passes on wear properties of Al-6061-T6 alloy. Journal of the Brazilian Society of Mechanical Sciences and Engineering. 2021; 43.
9. Cui GR, Ma ZY, Li SX. The origin of non-uniform microstructure and its effects on the mechanical properties of a friction stir processed Al-Mg alloy. Acta Materialia. 2009; 57: 5718-5729.
10. Frigaard Ø, Grong Ø, Midling OT. A Process Model for Friction Stir Welding of Age Hardening Aluminum Alloys. Metallurgical and Materials Transactions A. 2001; 32: 1189-1200.
11. Frigaard Ø, Grong Ø, Bjørneklett B, Midling OT. Modelling of the Thermal and Microstructural Fields During Friction Stir Welding of Aluminum Alloys. Proceeding 1st International Symposium on Friction Stir Welding, The Welding Institute, TWI; 1999 June; Thousand Oaks, CA, Cambridge, United Kingdom
12. Murr LE, Flores RD, Flores OV, McClure JC, Liu G, Brown D. Friction-stir welding: microstructural characterization. Materials Research Innovations. 1998; 1: 211-223.
13. Scialpi A, De Filippis LAC, Cavaliere P. Influence of shoulder geometry on microstructure and mechanical properties of friction stir welded 6082aluminium alloy. Materials & Design. 2007; 28:1124–1129.
14. Woo W, Choo H, Brown DW, Vogel SC, Liaw PK, Feng Z. Texture analysis of a friction stir processed 6061-T6 aluminum alloy using neutron diffraction. Acta Materialia. 2006; 54: 3871–3882.
15. Svensson LE, Karlsson L, Larsson H, Karlsson B, Fazzini M, Karlsson J. Microstructure and mechanical properties of friction stir welded aluminium alloys with special reference to AA 5083 and AA 6082. Science and Technology of Welding and Joining. 2000; 5: 285–296.
16. Hassan KAA, Prangnell PB, Norman AF, Price DA, Williams SW. Effect of welding parameters on nugget zone microstructure and properties in high strength aluminium alloy friction stir welds. Science and Technology of Welding and Joining. 2013; 8:257–268.
17. Mishra RS, Mahoney MW. Friction Stir Welding and Processing. ASM International: American Society of Material; 2007.
18. Pareek M, Polar A, Rumiche F, Indacochea JE. Mechanical properties and corrosion resistance of friction stir welded AZ31B-h24 magnesium alloy. Proc. 7th International Conference on Trends in Welding research; 2005; USA.
19. Chang CI, Lee CJ, Huang JC. Relationship between grain size and Zener-Holloman parameter during friction stir processing in AZ31 Mg alloys. Scripta Materialia. 2004; 51: 509–514.
20. Mirzadeh H. Simple physically-based constitutive equations for hot deformation of 2024 and 7075 aluminum alloys. Transactions of Nonferrous Metals Society of China. 2015; 25: 1614-1618. DOI:10.1016/S1003-6326(15)63765-7.
21. Humphreys JE. Recrystallization and Recovery. Materials Science and Technology. 2006: 373-398.
22. Harris D, Norman AF. Properties of Friction Stir Welded Joints. A Review of the Literature, EUROSTIR; 2003. Progress report presented at the 6th PSG Meeting.
23. Scialpi A, De Giorgi M, De Filippis LAC, Nobile R, Panella FW. Mechanical analysis of ultra-thin FSW joined sheets with dissimilar and similar materials. Materials & Design. 2008; 29:928–936.
24. Grong O, editor. Metallurgical modelling of welding. The Institute of Materials, London; 1997.
25. Moreira PMGP, Santos T, Tavares SMO, Richter-Trummer V, Vilaça P, de Castro PMST. Mechanical and metallurgical characterization of friction stir welding joints of AA6061-T6 with AA6082-T6. Materials & Design. 2009; 30:180–187.